PHIL simulation of a parallel HEV equipped with different energy storage systems

JUNYI LIANG, JIANLONG ZHANG, CHENGLIANG YIN，FUTANG ZHU
National Engineering Laboratory for Automotive Electronic Control Technology
Shanghai Jiao Tong University
800 Dongchuan Road, Minhang District, Shanghai,
CHINA
Junyi.LiangSH@gmail.com

Abstract: - Simulation has been acknowledged as an effective method of optimizing fuel consumption and sizing components for hybrid electric vehicles (HEVs). However, the accuracy of simulation results requires validation. Power-hardware-in-the-loop (PHIL) simulation can be an effective technique in obtaining accurate results and comparing different options before prototyping. Using the PHIL concept, this paper presents an implementation of a parallel HEV architecture on a dynamometer power train system. Four different energy storage systems (ESSs) in the HEV were tested to compare the performance of each system. The four ESSs included the battery-only type and the battery/ultra capacitor-based hybrid type. A fuzzy logic energy management strategy was implemented to address the power distribution in the HEV. In this paper, we compare and discuss the energy efficiency, electrical performance of the ESSs, and fuel economy of the HEV. The results show that hybrid ESSs have several advantages over the battery-only systems.

Key-Words: - Hardware-in-the-loop, Hybrid electric vehicle, Energy Storage System, fuzzy logic

1 Introduction

Requirements in developing clean and efficient vehicles have increased significantly. The increase has resulted from more stringent regulations for emissions and higher fuel prices. Pure electric vehicles (PEVs), hybrid electric vehicles (HEVs), and fuel cell vehicles (FCVs) have been proposed as replacements for conventional vehicles in the future [1]. Among the three types of vehicles, the HEV is transitional, more familiar to the public, and has been available in the market since the past decade.

To regulate the workload of the internal combustion engine (ICE), one or more electric motors (EMs) are added to the different types of commercial HEVs. Energy storage systems (ESSs) that supply the electrical power needed by EMs become the key components in successful implementation of HEVs [2-4]. In the past decade, different types of batteries have been applied as ESSs in HEVs [5-7]. Batteries typically contain reasonable or good energy density. However, compared with ideal energy storage components [2, 8], batteries have various limitations such as low power density, short lifecycle, and poor performance under low temperature. Table 1 presents the characteristics of certain energy storage components.

Table 1. Features of different energy storage components

Type	Energy density(Wh/kg)	Power density(W/kg)
Lead acid	40	100
Nickel-Metal Hydride	80	700
Li-ion	150	900
Ultra capacitor	5.6	11000

As shown in Table 1, the ultra capacitor (UC) has higher power density than other batteries. However, the energy density of the UC is considerably low. By combining the different features of batteries and UC, we can form a hybrid ESS (HESS) to ensure good performance in both energy density and power density [9-14].

The different ESS topologies as well as variable types and sizes of other power components, provide a high freedom to design a desired HEV. Simulation has been recognized as a good solution to address the diversity in designing HEVs. Various software products based on system modeling are specialized in the simulation of HEVs. The software products

efficiently provide different fuel economy results according to different HEV architectures [15-17].

Nevertheless, it is still difficult to obtain the actual performance of the key components through simulation. If the energy management strategy (EMS) performance strongly depends on the parameters of the key components, then the accuracy of the simulation results requires further verification.

Prototyping of the target HEV can provide accurate and final results, but it is an extremely costly solution for researchers. Power-hardware-in-the-loop (PHIL) is an interesting choice to obtain more accurate performance than pure simulation. Meanwhile, the PHIL simulation has lower cost requirement than prototyping [18-19]. Some of the real components can be tested on a bench by using the PHIL simulation. The real components receive the commands that are sent from the real-time simulation processor. Through installed sensors, the states of the real components also feed back to the real-time simulation processor.

In this paper, we highlight how the PHIL concept is implemented to test a parallel HEV architecture particularly with different ESSs. PHIL can be advantageous in changing different components (ESSs in this case) in similar configuration and driving conditions. Four different ESSs, namely, LiFePO4 battery, lead–acid battery, and their respective integrations with UC to form another two HESSs (Li-HESS and LA-HESS), are tested in the PHIL-parallel HEV configuration. According to the different topologies, the performances of the ESSs are compared in terms of the variation of current, voltage, and energy efficiency. A fuzzy-logic-based EMS is also introduced to address the power distribution between a battery and a UC in the HESS.

This paper is organized as follows. In Section 2, the base architecture of the target HEV and its features are presented. Section 3 describes the energy management system for the target HEV equipped with HESS by using fuzzy logic. Section 4 presents the PHIL simulation system that is mainly formed by a five dynamometers test bench, additional components, and real-time controllers. To demonstrate the different performance and energy efficiency of the ESSs, Section 5 presents detailed experimental results. Lastly, a brief conclusion is presented. Moreover, as direction of our future research, artificial intelligence techniques such as agent based modeling[20] will be employed in the modeling of the energy storage components.

2 Power architecture

The target HEV we have developed is mainly aimed at the mid-range and low-end vehicle markets. Considering the target markets and potential consumers, the target HEV has special features compared with other commercially available HEVs. First, the target HEV has small size and light weight. The HEV can also achieve low fuel consumption and is suitable for use in a crowded urban area. Second, the HEV mainly operates in urban and suburban districts and rarely runs on the highway, which reduces its maximum velocity. Finally, it is mainly used for commuting or driving in scenic areas, such that the driving distance is not long and acceleration demand is not high. As a result, powerful components need not be applied in the target HEV. To meet the aforementioned requirements, the kinetic performance of the target HEV is shown in Table 2 [21].

Table 2. Kinetic performance of target HEV

Item	Value
Maximum velocity(km/h)	⩽80
0-50km/h acceleration time(s)	⩽20
Grade-ability (%)	⩾20

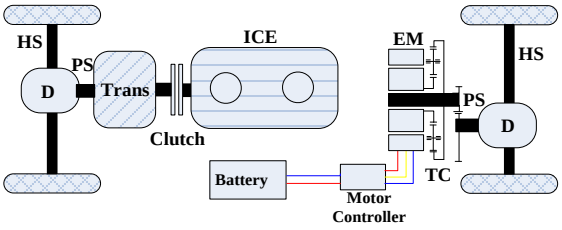

a) Adopting battery

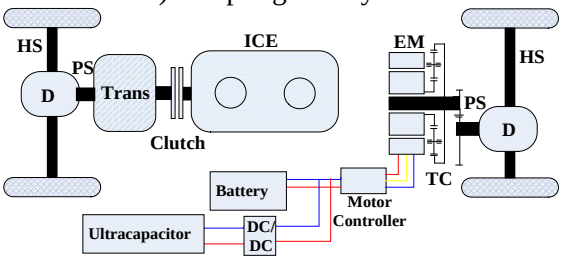

b) Adopting HESS

Fig. 1 Architecture of the target HEV power train

Figure 1 presents the two architectures of the target HEV with different ESS topologies. Figure 1(a) illustrates the adoption of the battery (lead–acid battery and LiFePO4 battery in this study), and Figure 1(b) illustrates the adoption of the Li-HESS or LA-HESS. A double-cylinder engine with small displacement at the front drive axle was adopted. The double-cylinder engine was connected to the

automatic manual transmission (AMT). The output shaft of the AMT was linked to the propeller shaft (PS), differential, half shafts, and two wheels. At the rear drive axle, the electric motor (EM) was connected to the PS through a torque coupler (TC). The TC increases the working speed of the EM by applying a 5.187 gear ratio. By applying the gear ratio, the operating range of the electric motor is ensured so that it can match the maximum speed constraint and power requirement of the vehicle. In this configuration, the HEV can easily switch between two-wheel drive mode and four-wheel drive mode based on the road and operating conditions. Moreover, cancelling Integrated Starter Generator can also reduce the cost of the HEV.

The HESS is composed of a battery pack, a UC pack, and a bi-directional DC/DC converter. The UC pack connects with the battery pack through the bi-directional DC/DC converter. The energy density of the battery is relatively high, but the transient power response of the battery is not desirable. When the discharge rate is high, the heat of the battery increases. The increased heat increases the temperature of the battery pack, which results in low cell efficiency. The heat also deteriorates the safety and life cycle of the battery. By contrast, the energy density of the UC is low whereas the power density is considerably high. The UC can meet the instantaneous high power demand of the EM. By combining the two types of electrical sources, the battery only has to meet the average electrical power requirement during HEV driving. The UC is used to make up for the fluctuations in electrical power demand. Combining the two types of electric sources mitigates the battery workload. The combination also helps to improve the working efficiency and prolong the life expectancy of the battery. Because of the high power density of the UC, the HESS can better absorb the regenerated power during vehicle regenerative braking. As a result, the HESS can be expected to have better energy efficiency than the traditional ESS.

Table 3 lists the specifications of the target HEV. A small double-cylinder engine with 0.25 liter displacement was chosen as fuel converter. The electric motor is a permanent magnet brushless DC motor that can also regenerate power during engine driving or vehicle braking. We selected a 40 Ah and 72 V LiFePO4 battery pack, a 45 Ah and 72 V lead–acid battery pack, and a 48 V UC pack. The AMT parameters are also presented in Table 3.

3 Energy management strategy

3.1 Energy management topology

To address the complexity of the power train system (the target HEV equipped with HESS), we adopted an EMS that is mainly based on fuzzy logic. Several modes in the EMS are used, namely, pure electric mode (PEM), parallel mode (PM), and braking mode (BM). Depending on the driving conditions and component status of the vehicle, the HEV runs

Table 3. Specifications of the target HEV

Vehicle and components	Parameter	Value
Vehicle	Curb/Gross weight(kg)	850/1150
	Tire rolling radius(m)	0.28
	Frontal area(m2)	1.91
	Aerodynamic drag coefficient	0.34
	Rolling resistance coefficient	0.009
ICE	Idle/maximum speed(rpm)	1400/8000
	Maximum torque($N \cdot m$)	18.7/5500
	Maximum power(kW)	12.7/7000
	Displacement(l)	0.25
Traction motor	Peak power(kW)	14
	Continuous Power(kW)	7
	Peak torque($N \cdot m$)	70
LiFePO4 Battery	Capacity(Ah)	40
	Equivalent series resistance(ohm)	0.052
	Nominal operating voltage(V)	72
Lead-Acid Battery	Capacity(Ah)	45
	Equivalent series resistance(ohm)	0.084
	Nominal operating voltage(V)	72
Ultra capacitor	Capacitance(F)	165
	Nominal operating voltage(V)	48.6
	Emax (Wh/kg)	3.81
	Pmax (W/kg)	7900
Transmission Speed Ratios	1st gear	4.2
	2nd gear	2.408
	3rd gear	1.505
	4th gear	1
	Final Drive Ratio	5.187

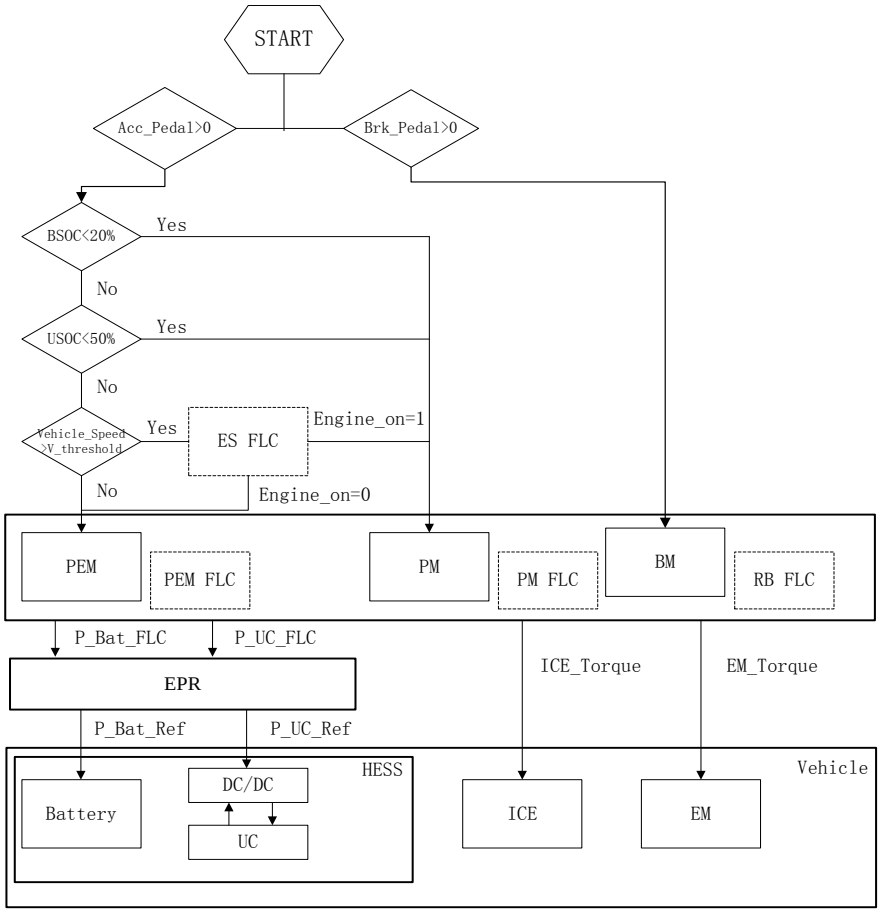

Fig. 2 EMS topology

in the three different modes. As shown in Fig. 2, the threshold constraints are adopted to decide the mode switching. The accelerator and brake pedal positions decide the HEV that runs in a driving or braking mode. To protect the battery and the UC, a 20% battery state of charge (BSOC) constraint and a 50% UC state of charge (USOC) constraint are adopted. When the BSOC or USOC drops below their constraints, the ICE must be switched on. The mode changes from PEM to PM. If both the BSOC and USOC are higher than their constraints, a vehicle speed threshold is adopted to allow starting the ICE. The ICE can be started after the rotating speed has entered the high-efficiency speed area. Nevertheless, the PEM is still preferred if the power request is low and the HESS can support sufficient power to meet the request. An engine status (ES) fuzzy logic controller (FLC) was constructed to handle this situation. Section 3.2.1 further explains the process for the FLC.

When the mode is decided, the related FLC handles the power distribution in each mode. Fig. 2 shows the ES FLC and the three other FLCs, which are PEM FLC, PM FLC, and regenerated braking (RB) FLC. By using the three FLCs, the ICE torque, the EM torque, the battery power, and the UC power can be decided and sent to the corresponding vehicle components.

An electrical power redistribution (EPR) module is found in the EMS. The FLCs distribute the power between the battery and the UC. However, the battery current can change beyond the constraints depending on the intrinsic features of the battery. Thus, EPR is introduced to limit the battery current in terms of level and slope. The battery current is then kept within an interval [maximum charge current (−3 C), maximum discharge current (3 C)] by employing a saturation model. Moreover, a "battery current slope limitation" [10] at a delay $F(s)$ is embedded in EPR to permit the safe operation of the battery, even during transient power demand. To obtain a natural linear transfer function, a second-order delay (filter) $F(s)$ is chosen for the battery current dynamics as follows:

$$F(s)=\frac{1}{(s/\omega_n)^2+(2\cdot\zeta/\omega_n)s+1} \quad (1)$$

where ω_n and ζ are the regulation parameters. Thus, a new battery power "P_Bat_Ref" can be obtained, and the power command "P_UC_Ref" sent to the DC/DC converter can also be acquired.

By employing the EPR, the battery load can be mitigated, and the transient fluctuations of electrical power can be met by the UC.

3.2 Fuzzy logic controllers

The fuzzy logic control has been applied successfully to the design of the HEV control strategy [22–29]. In this study, we use four controllers that employ fuzzy logic in the EMS. The four controllers are ES FLC, PEM FLC, PM FLC, and RB FLC. The ES FLC decides which mode should be operated. The PEM FLC distributes the requested power in the HESS in PEM. The PM FLC conducts the power distribution between the ICE and EM. The RB FLC handles the distribution of the absorbed energy from regenerative braking. The four controllers cooperate with one another to satisfy the energy management requirements of the target HEV.

3.2.1 ES FLC

Under driving condition, the ES FLC decides which mode should be employed. Normally, PM is preferred when the EM torque is insufficient to meet the driver power demand or if the battery SOC is too low. However, the most common reason for switching to PM is that: the driver power demand is higher than the power threshold that the ICE has to be switched on.

As the deep charge and discharge cycles affect the battery lifetime [30], keeping the battery operating in a narrow BSOC range provides better protection. To maintain the BSOC, the ES FLC was constructed. The ES FLC addresses the relationship between the ICE ON command and the current BSOC. As shown in Fig. 3 [31], the ICE was turned OFF below a certain electric launch speed when the BSOC was not extremely low. Above the limited speed, the ICE would be turned ON if the required ICE torque was higher than the off torque envelope (OTE) at the current speed. The MS FLC was used to relocate the OTE based on the current SOC. The OTE would move up or down when the BSOC changed. Thus, the OTE would let the ICE be turned ON “earlier” or “later” to meet the charge-sustaining request. If the BSOC was extremely low (e.g., lower than the 20% BSOC constraint), the ICE would not be shut down.

The structure of the fuzzy logic controller is presented in Fig. 4. The decisions of the ES FLC are based on the departure of the current BSOC from the target BSOC. The changes in the rate of the BSOC also affect the decisions of the ES FLC. Multiplied by a conversion coefficient, the ES FLC can output the offset torque from the original threshold. The offset torque is compared with the required ICE torque to decide whether the PM should be selected. Fig. 5 shows the fuzzy surface of the ES FLC.

3.2.2 PEM FLC

The PEM FLC is specifically designed for the energy flow control in the PEM. Fig. 6 presents the block diagram of the PEM FLC. The inputs of the FLC are the required power from the EM (P_EM), BSOC, and USOC.

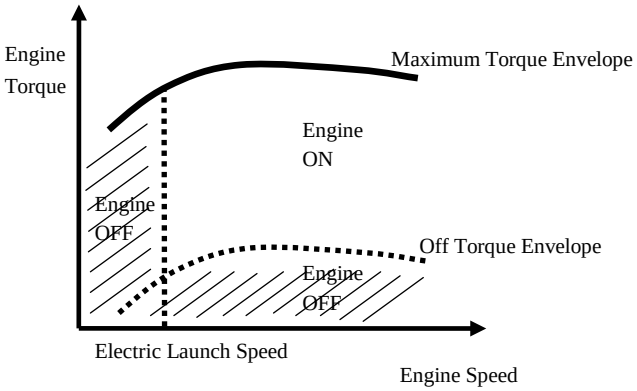

Fig. 3 Engine ON/OFF threshold

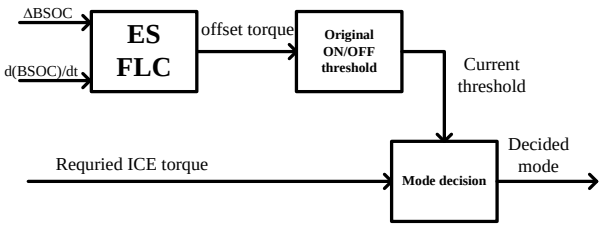

Fig. 4 Block diagram of ES FLC

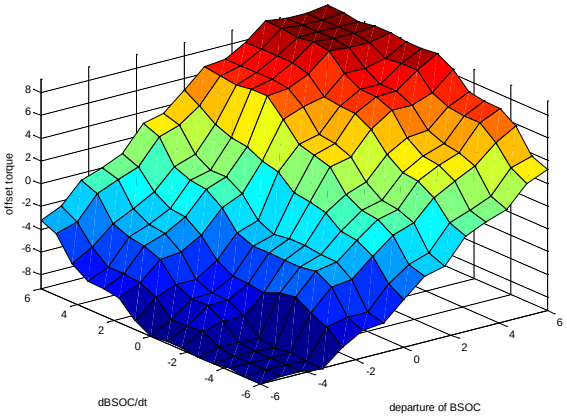

Fig. 5 Fuzzy surface of ES FLC

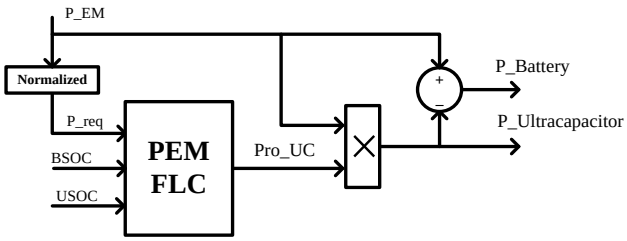

Fig. 6 Block diagram of PEM FLC

The PEM FLC output is indicated as Pro_UC, which means that the proportion of the P_EM is supplied by the UC. The rest of the P_EM is supplied by the battery. The UC can meet high power and large current requirement in a short time. However, the energy density of the UC is significantly lower than that of the battery. The battery is a good energy storage component that can provide electric energy for longer time than UC. According to the different energy and power features of the UC and battery, a proper fuzzy logic for the PEM can be established. The battery provides the total electric energy if the USOC is low and the power requirement of the motor is not extremely high. Otherwise, the requirement is met by both the UC and the battery. The energy distribution between the battery and the UC is decided by their SOC status and the operation power of the motor. Fig. 7 illustrates the fuzzy surface of the PEM FLC.

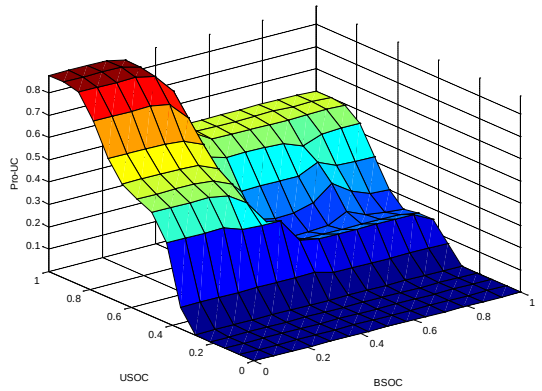

Fig. 7 Fuzzy surface of PEM FLC

3.2.3 PM FLC

The PM is the "full" mode that employs both ICE and EM to work together for the HEV. Fig. 8 presents the block diagram of the proposed PM FLC. The PM FLC has three inputs and one output. The inputs of the PM are the ICE speed (IS), accelerated pedal position (K), and BSOC. The output is the Tice which represents the torque percentage of the maximum engine torque at the current rotational speed. Notably, a value of 0.5 for Tice indicates the highest efficiency operation torque of ICE, which will change according to the ICE speed.

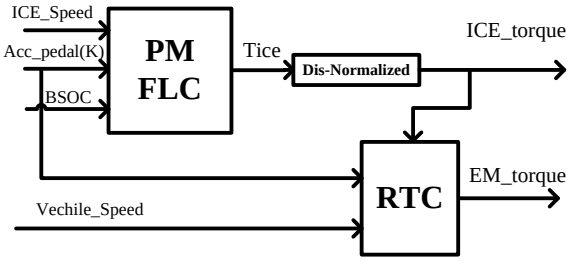

Fig. 8 Block diagram of PM FLC

Given that the energy stored in the battery is significantly larger than that in the UC, the PM FLC mainly regulates the BSOC level by adjusting the ICE torque. The PM FLC intends to control the ICE to operate in a comparatively high-efficiency region. To keep the BSOC at a normal range, the torque command of the ICE can be tuned. If the BSOC is high, the ICE power drops and the EM provides more power. If the BSOC is low, additional power is provided by the ICE to charge the battery. Given that the PM FLC only distributes power between the ICE and the EM, power management of the HESS requires cooperation among the PM FLC and other FLCs. When the PM FLC outputs a positive power command to the EM, the HESS has to output power for EM-assisted driving. Then, the PEM FLC is called to regulate the output power flow between the battery and the UC. When the EM regenerates power to charge the HESS, the RB FLC (as discussed in Section 3.2.4) meets the regenerative power distribution requirement. Fig. 9 illustrates the fuzzy surface of the PM FLC.

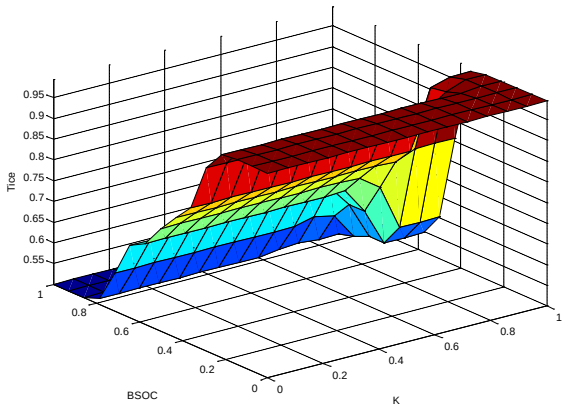

Fig. 9 Fuzzy surface of PM FLC

3.2.4 RB FLC

The RB represents the regenerative braking condition. Fig. 10 shows the block diagram of the proposed FLC for the RB. The inputs of the FLC are

BSOC and USOC. The RB mainly distributes the regenerative energy between the battery and the UC. With high dynamic performance, the UC should be first charged by the large current when HEV breaks in a hard transient state. When the USOC is low, the UC receives more RB power. When the USOC is high, the battery receives more RB power. Fig. 11 presents the fuzzy surface of the RB FLC.

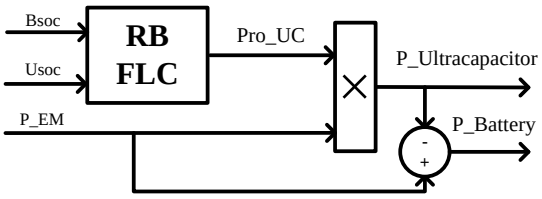

Fig. 10 Block diagram of RB

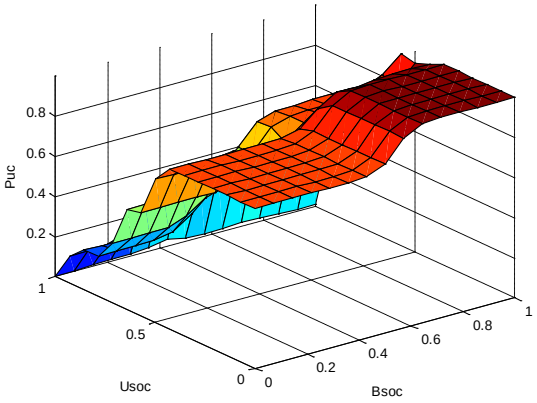

Fig. 11 Fuzzy surface of RB FLC

4 PHIL system design

The PHIL control for the parallel HEV configuration was implemented on a dynamometer power train system (DPS). As shown in Fig. 12, the DPS consists of four AC Motors as outputs and 1 AC motor as input. The input/output AC vector motors are in conjunction with vector drives. Compared with the DC motor and drive systems, the input/output AC vectors lend better motor durability, faster response time, are smaller, and have better power generation at high speeds. Table 4 lists the specifications of the motors.

Table 5. The specifications of dynamometer motors

Motors	Type	Speed	Torque
Input motor	280kW AC vector motor	0~8000rpm (Bi-direction)	453Nm (From 0 to 5900rpm)
Front output motor	170kW AC vector motor	0~3000rpm (Bi-direction)	2029Nm (From 0 to 800rpm)
Rear output motor	380kW AC vector motor	0~2500rpm (Bi-direction)	4535Nm (From 0 to 800rpm)

The control system for the DPS was grouped based on three major parts: iTest, Procyon, and Unico Drive. iTest is the central control and data acquisition system in the DPS. iTest executes a predefined test schedule which is the Economic Commission of Europe (ECE) driving cycle in the test. The test involves coordinating the dynamometers along with data acquisition from the sensors on the test articles and in-cell instruments. Procyon is a real-time platform for control algorithm prototyping and PHIL simulation testing. In our test, iTest and Procyon were assembled in the control cabinet and were connected to each other via the User Datagram Protocol bus (see Fig. 13). Unico Drive was integrated with the dynamometers in the DPS. Unico Drive controlled the dynamometers to ensure accurate behavior during the test.

Fig. 12 The dynamometer power train system

Fig. 13 The control cabinet of the DPS

Fig. 14 The AV900 power system

In the test, a bi-directional multi-channel DC power system called AV900 was adopted to simulate the ESS. As shown in Fig. 14, the AV900 can provide or absorb electric energy that the EM consumes or regenerates. Fig. 15 illustrates the AV900 and EM system assembled with the DPS to match the architecture of the target HEV. The input motor 0 connects with the AMT. The output motors 1 and 2 simulate the front wheels. Both input and outputs are used as the front axle power train of the target HEV. The ouput motor 3 and 4 simulate the rear wheels. The AV900 and EM system are integrated in the rear axle power train. By using the power from AV900, the EM can drive the output motors 3 and 4 alone.

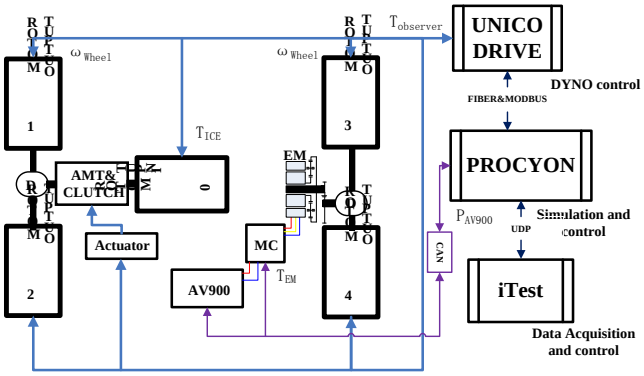

Fig. 15 HEV Power train DYNO Control System Architecture

The engine torque map data of the objective double-cylinder engine is downloaded into the models in Procyon. Then, the controller sends the torque command T_{ICE} to the AC drive of the input motor. The input motor runs as a virtual engine in this test. The parameters of the target HEV are imported into the models by using the graphical user interface (GUI). Through the GUI, the models can simulate the resistance of the HEV that has to be overcome under the ECE driving cycle.

The FLCs and vehicle component models built in Matlab/Simulink are downloaded into Procyon. Then, Procyon works as a virtual HEV controller to communicate with all of the power sources. Procyon uses a controller area network bus to communicate with the additional motor controller and AV900, sending motor torque command T_{EM} to the former and receiving real time power signal P_{AV900} from the latter. Procycon also uses original fiber optic to communicate with the Unico Drive, sending torque T_{ICE} and speed command ω_{Wheel} to the corresponding Dynos. Then, the observed torque values $T_{observer}$ on motors 1 to 4 are transmitted to Procyon as the actual torque values on the wheels. With the power signal P_{AV900} from the AV900, Procyon can calculate and output the power requirements to the ESS. By using all of the software and hardware configurations, the construction of a closed-loop test environment that simulates the real HEV road test is accomplished.

5 Results

The PHIL test results are presented in this section. The driving cycle used for the fuel economy evaluation is the ECE driving cycle. Table 5 lists the characteristic parameters of the ECE driving cycle.

Table 5. ECE driving cycle

Parameter	Value
Time(s)	800
Distance(km)	4.052
Maximum speed(km/h)	50
Average speed(km/h)	18.234
Maximum acceleration(m/s2)	1.043
Maximum deceleration(m/s2)	-0.926
Idle time percentage (%)	32

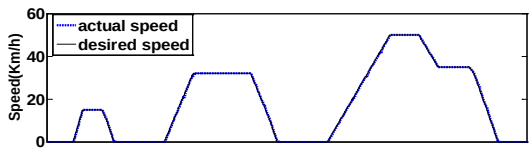

(a) Comparison of the actual and desired speed

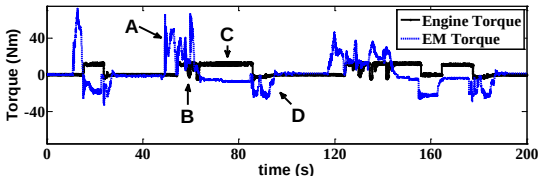

(b) The engine and EM torque

Fig. 16 Test results of speed and torque of the target HEV under ECE driving cycle

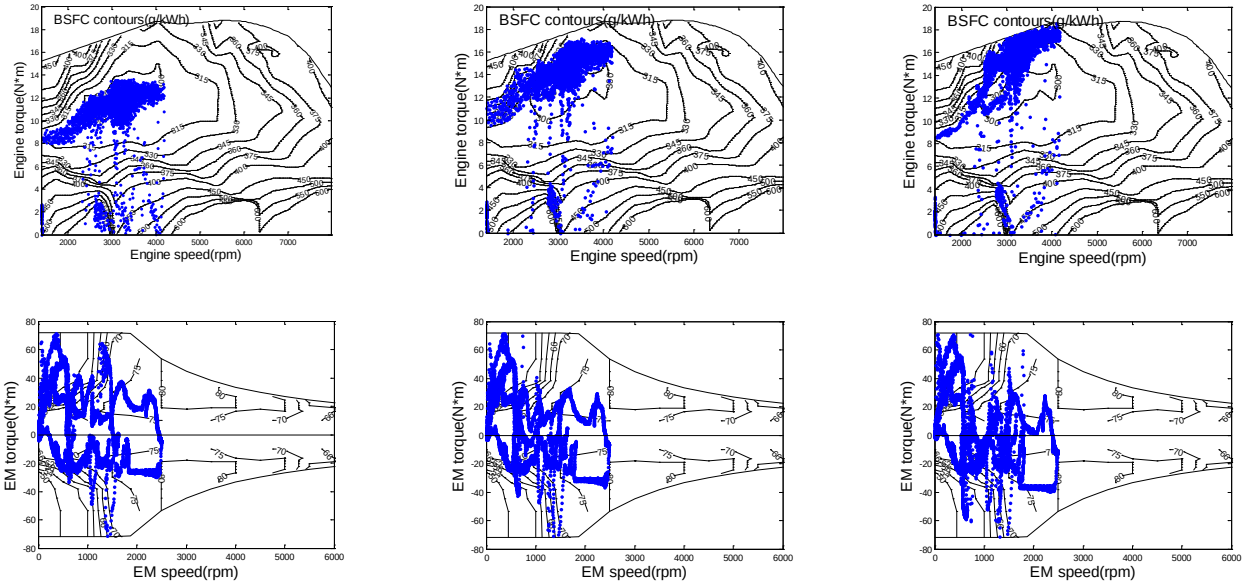

(a) Initial BSOC = 70% (b) Initial BSOC = 50% (c) Initial BSOC = 30%

Fig. 17 The engine and EM working points with different initial BSOC values

As shown in Fig.16, the actual speed can follow the desired speed well, demonstrating the kinetic performance of the target HEV can meet the specific usage condition as we introduced in section 2. The mode transition is also presented in Fig. 16. “A” represents the PEM and the EM that drives the HEV alone. When the vehicle speed is higher, the propelling mode changes from “A” to “B”, the motor assistant condition in the PM and ICE drives the HEV along with the EM. Then, the vehicle speed reaches a constant value and the mode changes to “C”, which is the parallel charge condition is in the PM.

The engine works in the high-efficiency area and the additional power is used to drive the EM to charge the ESS. Then, the mode changes to “D” (RB) when the driver depresses the brake pedal. The EM regenerates the braking power to charge the ESS, thereby improving the overall energy utilization efficiency.

Fig. 17 illustrates the engine and EM working points under different initial BSOC values. When the BSOC is 70%, the fuzzy logic controller leads the engine to work in the highest-efficiency area (see Fig. 17(a)). Meanwhile, the EM can work with the engine to meet the power requirement. Fig. 17(b) shows that if the initial BSOC of 50% is slightly lower than the normal SOC working area of the battery, the engine working points move to a higher torque area to provide more power and charge the battery. As shown in Fig. 17(c), when the initial BSOC is extremely low at 30%, the engine working points move to the highest torque area and charge the battery immediately to keep the battery healthy. These results demonstrated that EMS can regulate power sources to cooperate well to guarantee the balance of the BSOC.

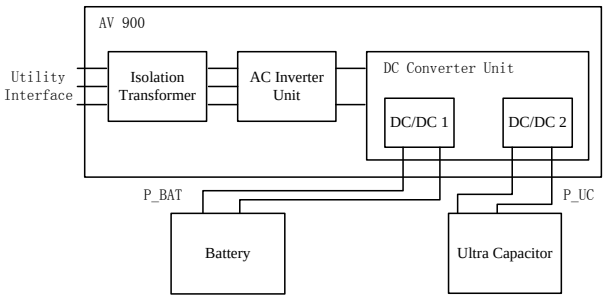

Fig. 18 Topology of the HESS test

As discussed in Section 4, the AV900 was adopted to simulate the ESS in the test bench. According to the EM power consumption in AV900, the EMS can output distributed power requirements for battery/UC in HESS simultaneously during the ECE driving cycle. Then, the distributed power requirements are loaded to the real battery and the UC by AV900 to test and verify the effectiveness of the proposed EMS. Fig. 18 shows the topology of the HESS test. The battery and the UC are connected to AV900 with different DC/DC converters. Then, the AV900 works in power mode

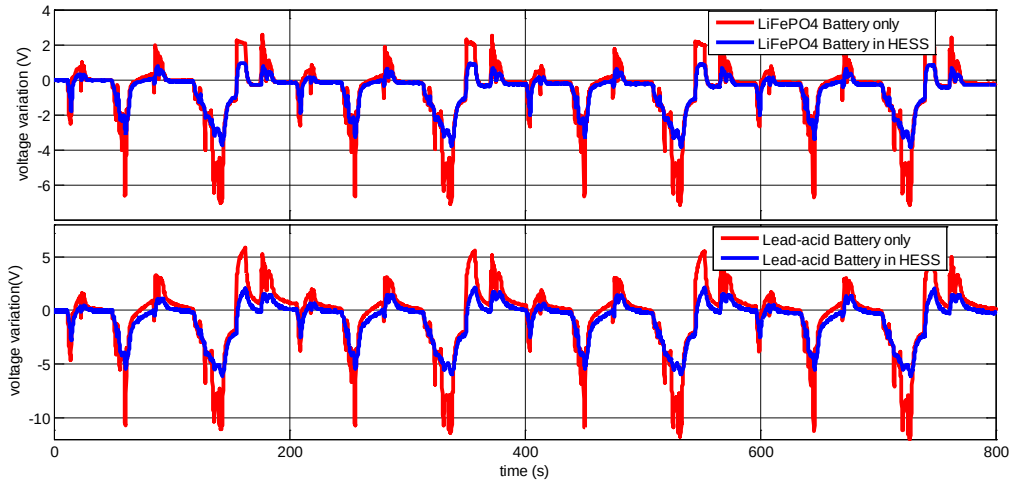

Fig. 19 Voltage variation of the batteries in four ESS topologies

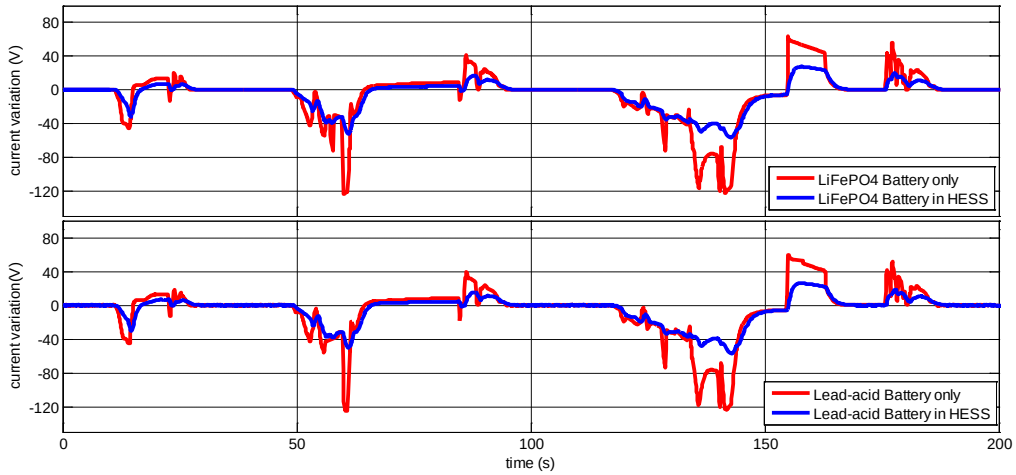

Fig. 20 Current variation of the batteries in four ESS topologies

Table 6 Voltage variation of the batteries in four ESSs

Voltage	Maximum voltage(V)	Minimum voltage(V)	Fluctuation range(V)	The percentage of decrease
Lead-acid battery only	81.06	63.24	17.82	0%
Lead-acid battery in HESS	76.8	68.52	8.28	53.53%
LiFePO4 battery only	75.16	65.44	9.72	0%
LiFePO4 battery in HESS	73.6	68.74	4.86	50%

Table 7 Current variation of the batteries in four ESSs

Current	Maximum current(A)	Minimum current(A)	Fluctuation range(A)	The percentage of decrease
Lead-acid battery only	-127.34	62.08	189.42	0%
Lead-acid battery in HESS	-56.72	26.82	83.54	55.90%

LiFePO4 battery only	-124.38	66.14	190.52	0
LiFePO4 battery in HESS	-56.7	27.52	84.22	55.79%

Table 8. Energy efficiency results of four ESSs

		Lead-acid Battery Only	LA-HESS	LiFePO4 Battery Only	Li-HESS
BSOC	Initial (%)	70	70	70	70
	Final (%)	67.41	67.78	67.21	67.52
UC voltage	Initial (%)	/	45.6	/	45.6
	Final (%)	/	41.65	/	41.76
Battery energy Consumption (Wh)		87.03	74.70	80.82	71.90
UC energy Consumption (Wh)		/	5.92	/	5.76
Total energy Consumption (Wh)		87.03	80.62	80.82	77.66
Energy efficiency improvement by adopting HESS (%)		/	7.36	/	3.91
Total energy saving (%)		0	7.36	7.14	10.77

to load the separate power commands to the battery and the UC. By connecting the LiFePO4 battery and the lead–acid battery to the AV900 separately, the battery-only system test is also conducted. The results are discussed as follows. Fig. 19 shows that in the battery-only system, the voltage variations of batteries are relatively large. The large voltage variations may increase the control difficulty of the EM system. The voltage variation of the lead–acid battery is particularly larger than that of the LiFePO4 battery because of the higher internal resistance of the former. By contrast, the voltage variations of both the LiFePO4 battery and the lead–acid battery decreased significantly when the batteries were integrated in the HESS topology. As summarized in Table 6, the fluctuation range of the direct current (DC) link voltage in the HESSs is reduced approximately 50% than that of the battery-only systems.

Fig. 20 illustrates the current variations of the four ESSs. Research showed that large and rapid fluctuant current is harmful to the battery health and can deteriorate the battery life expectancy [32]. Compared with the almost 3 C current fluctuation in the battery-only system, the current fluctuation of the battery in the HESS has dramatically decreased to approximately 1.5 C. As summarized in Table 7, the current fluctuations decreased by approximately 55% in both HESSs.

Table 8 presents the energy efficiency results of the four ESSs. Given the different intrinsic features, the lead–acid battery consumed more energy than the LiFePO4 battery when meeting the same power requirement. By integrating the battery with the UC in HESS, both the energy efficiency of the LA-HESS and the Li-HESS were improved. The efficiency improvement of the LA-HESS was larger than that of the Li-HESS. However, the Li-HESS showed the best performance in total energy consumption. Considering the cost factor, the LA-HESS could be a choice. However, the lead–acid battery in the LA-HESS could be a potential source of pollution [2].

Based on the different performances in voltage, current, and energy efficiency of the four ESSs, the following conclusions can be made:

1) By integrating the battery and the UC in the HESS, the voltage fluctuation on the DC link was decreased, which facilitate us to control the EM system. Among the four ESSs, the Li-HESS had the lowest voltage fluctuation thus the Li-HESS was the best in cooperating with the EM system.

2) The current fluctuation of the battery decreased in the HESSs than in the battery-only system. The decrease mitigated the workload of the battery, which could result in longer battery life.

3) The energy consumption decreased when the HESS topology was used. Both the LA-HESS and Li-HESS exhibited better performance than the

battery-only systems. The Li-HESS had the best energy efficiency result among the four ESSs.

Given that the Li-HESS had the best energy efficiency among the four ESSs, we chose the topology of the HEV equipped with Li-HESS to evaluate the fuel consumption of the HEV. By downloading the fuel consumption map of the ICE into Procyon, the fuel consumption of the ICE in the ECE driving cycle was calculated. Under the ECE driving cycle, electrical energy consumption in the HESS occurred. Given the difficulty to obtain perfect zero electrical energy consumption in an experiment, we conducted several experiments with different initial HESS status. Then, a linear interpolation method was employed to estimate the total fuel consumption at the zero electrical energy consumption point. Fig. 21 indicates that the estimated fuel consumption was improved to 23% compared with the average reference vehicle consumption values.

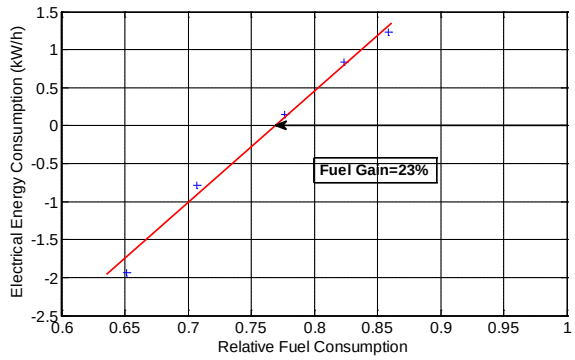

Fig. 21 Relative fuel consumption of the HEV equipped with Li-HESS

4. Conclusion

In this study, a parallel HEV configuration was applied in a DPS by using the PHIL technique. We provided a detailed implementation of the PHIL approach in the DPS. An EMS based on fuzzy logic was developed and adopted in the control system to manage the energy flow of the entire power train.

Four different ESSs, namely, LiFePO4 battery, lead–acid battery, Li-HESS, and LA-HESS, were tested and compared with the similar vehicle parameters and experimental conditions. By combining the high energy density feature of the battery and the high power density feature of the UC, the HESS showed several advantages compared with the battery-only system. The HESS could significantly release the battery workload, which resulted in longer life expectancy of the battery. The voltage variation in the DC link was also reduced. The reduction was beneficial for the EM system control. The energy efficiency of the HESSs was higher than that of the corresponding battery-only systems. The LA-HESS had a cost advantage compared with the Li-HESS. However, the LA-HESS could be a potential source of pollution. The Li-HESS exhibited the best performance among the four ESSs.

In-depth understanding of the optimal operation of the HESS can further improve system efficiency and maintain the health of electric components. Optimal operation of the HESS remains a significant issue that requires further investigation.

References:

[1] Ehsani, M, Y. Gao, and A. Emadi, *Modern Electric, Hybrid Electric, and Fuel Cell Vehicles*. 2009: CRC Press.

[2] C. Chan, L. Sun, R. Liang, and Q. Wang, Current status and future trends of energy storage system for electric vehicles. *Journal of Asian Electric Vehicles*, 2007. 5(2): p. 1055-1060.

[3] W. W. Xiong, and C. L. Yin, Design of series-parallel hybrid electric propulsion systems and application in city transit bus. *WSEAS Transactions on Systems*, 2009. 8(5): p. 578-590.

[4] Z. W. Wu, Z. L. Zhang, C. L. Yin, and Z. Zhao, Design of a soft switching bidirectional DC-DC power converter for ultracapacitor-battery interfaces. *International Journal of Automotive Technology*, 2012. 13(2): p. 325-336.

[5] D. Y. Jung, B. H. Lee, and S. W. Kim, Development of battery management system for nickel–metal hydride batteries in electric vehicle applications. *Journal of Power Sources*, 2002. 109(1): p. 1-10.

[6] Eckhard.Karden, Servé.Ploumen, Birger.Fricke, Ted.Miller, and Kent.Snyder, Energy storage devices for future hybrid electric vehicles. *Journal of Power Sources*, 2007. 168(1): p. 2-11.

[7] A.Vasebi, M. Partovibakhsh, and S.M.T. Bathaee, A novel combined battery model for state-of-charge estimation in lead-acid batteries based on extended Kalman filter for hybrid electric vehicle applications. *Journal of Power Sources*, 2007. 174(1): p. 30-40.

[8] Z. W. WU, J. L. Zhang, L. JIANG, H. J. WU, and C. L. YIN, The energy efficiency evaluation of hybrid energy storage system based on ultra-capacitor and LiFePO4 battery.

WSEAS TRANSACTIONS on SYSTEMS, 2012. 11(3): p. 95-105.

[9] F.S. Garcia,, A.A. Ferreira, and J.A. Pomilio, Control Strategy for Battery-Ultracapacitor Hybrid Energy Storage System. *Applied Power Electronics Conference and Exposition*, 2009. APEC 2009. Twenty-Fourth Annual IEEE. 2009.

[10] P. Thounthong, S. Raël, and B. Davat, Energy management of fuel cell/battery/supercapacitor hybrid power source for vehicle applications. *Journal of Power Sources*, 2009. 193(1): p. 376-385.

[11] A. Khaligh, and Z. H. Li, Battery, Ultracapacitor, Fuel Cell, and Hybrid Energy Storage Systems for Electric, Hybrid Electric, Fuel Cell, and Plug-In Hybrid Electric Vehicles: State of the Art. *IEEE Transactions on Vehicular Technology*, 2010. 59(6): p. 2806-2814.

[12] J. Cao, and A. Emadi, A New Battery/UltraCapacitor Hybrid Energy Storage System for Electric, Hybrid, and Plug-In Hybrid Electric Vehicles. *IEEE Transactions on Power Electronics*, 2012. 27(1): p. 122-132.

[13] J. Lopes, and J.C. Quadrado, Dual mode hybrid bus energy storage system. *WSEAS Transactions on Systems*, 2004. 3(5): p. 2170-2175.

[14] J. Y. LIANG, J. L. ZHANG, X. ZHANG, S. F. YUAN, and C. L. YIN, Energy management strategy for a parallel hybrid electric vehicle equipped with a battery/ultra-capacitor hybrid energy storage system. *Journal of Zhejiang University SCIENCE A*, 2013. 14(8): p. 535-553.

[15] A. Rousseau, P. Sharer, and M. Pasquier, Validation process of a HEV system analysis model: PSAT. *SAE paper*, 2001(2001-01): p. 0953.

[16] Tony. Markel, Aaron. Brooker, T. Hendricks, V. Johnson, et al, ADVISOR: a systems analysis tool for advanced vehicle modeling. *Journal of Power Sources*, 2002. 110(2): p. 255-266.

[17] F.Sangtarash, V. Esfahanian, H. Nehzati, et al, Effect of different regenerative braking strategies on braking performance and fuel economy in a hybrid electric bus employing CRUISE vehicle simulation. *SAE International Journal of Fuels and Lubricants*, 2009. 1(1): p. 828-837.

[18] R. Trigui, B. Jeanneret, B. Malaquin, and C. Plasse, Performance Comparison of Three Storage Systems for Mild HEVs Using PHIL Simulation. *IEEE Transactions on Vehicular Technology*, 2009. 58(8): p. 3959-3969.

[19] S. Kermani,R. Trigui, S. Delprat, B. Jeanneret, and T.M. Guerra, PHIL Implementation of Energy Management Optimization for a Parallel HEV on a Predefined Route. *IEEE Transactions on Vehicular Technology*, 2011. 60(3): p. 782-792.

[20] F. NERI, Quantitative Estimation of Market Sentiment: a discussion of two alternatives. *WSEAS Transactions on Systems, WSEAS Press (Athens, Greece)*, 2012. 11 (12): p. 691-702.

[21] L. Wang, Z. L. Zhang, C. L. Yin, Z. W. Wu, and Y. Zhang, Realization and Analysis of Good Fuel economy and Kinetic Performance of a Low-cost Hybrid Electric Vehicle. *Chinese Journal of Mechanical Engineering*, 2011.

[22] B. Baumann, G. Rizzoni, and G. Washington, Intelligent Control of Hybrid Vehicles Using Neural Networks and Fuzzy Logic.1998.

[23] N.J. Schouten, M.A. Salman, and N.A. Kheir, Energy management strategies for parallel hybrid vehicles using fuzzy logic. *Control Engineering Practice*, 2003. 11(2): p. 171-177.

[24] S. M. T. Bathaee, A. H. Gastaj, S. R. Emami, and M. Mohammadian, A fuzzy-based supervisory robust control for parallel hybrid electric vehicles. *Vehicle Power and Propulsion, 2005 IEEE Conference*. 2005.

[25] K. S. Jeong, W. Y. Lee, and C. S. Kim, Energy management strategies of a fuel cell/battery hybrid system using fuzzy logics. *Journal of Power Sources*, 2005. 145(2): p. 319-326.

[26] W. Jong-Seob, and R. Langari, Intelligent energy management agent for a parallel hybrid vehicle-part II: torque distribution, charge sustenance strategies, and performance results. *IEEE Transactions on Vehicular Technology*, 2005. 54(3): p. 935-953.

[27] R. Langari, and W. Jong-Seob, Intelligent energy management agent for a parallel hybrid vehicle-part I: system architecture and design of the driving situation identification process. *IEEE Transactions on Vehicular Technology*, 2005. 54(3): p. 925-934.

[28] W. W. Xiong, Y. Zhang, and C. L. Yin, Optimal energy management for a series–parallel hybrid electric bus. *Energy Conversion and Management*, 2009. 50(7): p. 1730-1738.

[29] A. A. Abdelsalam, and S. Cui, A Fuzzy Logic Global Power Management Strategy for Hybrid Electric Vehicles Based on a Permanent Magnet Electric Variable Transmission. *Energies*, 2012. 5(4): p. 1175-1198.

[30] E. Schaltz, A. Khaligh, and P. O. Rasmussen, Influence of Battery/Ultracapacitor Energy-Storage Sizing on Battery Lifetime in a Fuel Cell Hybrid Electric Vehicle. *IEEE Transactions on Vehicular Technology*, 2009. 58(8): p. 3882-3891.

[31] H. J. Valerie, B. W. Keith, and J. R. David, HEV Control Strategy for Real-Time Optimization of Fuel Economy and Emissions. *SAE Technical Paper* 2000-01-1543, 2000.

[32] H. L. CHEN, X. P. QIU, W. T. ZHU, and P. Hagenmuller, Synthesis and high rate properties of nanoparticled lithium cobalt oxides as the cathode material for lithium-ion battery. *Electrochemistry Communications*, 2002. 4(6): p. 488-491.